J Mol Model (2013) 19:3603–3610
DOI 10.1007/s00894-013-1895-8

ORIGINAL PAPER

Oxygen doped SiC nanocrystals: first principles study of the optical properties

Masoud Bezi Javan

Received: 14 March 2013 / Accepted: 21 May 2013 / Published online: 7 June 2013

Abstract We have studied a typical spherical SiC nanocrystal with a diameter of 1.2 nm ($Si_{43}C_{44}H_{76}$) using linear combination of atomic orbitals in combination with pesudopotential density functional calculation. The role of fluorine and oxygen impurities was investigated on the electronic and optical properties of the $Si_{43}C_{44}H_{76}$ nanocrystal. Total energy calculations show that the fluorine doped $Si_{43}C_{44}H_{76}$ nanocrystals are unstable. Oxygen doped $Si_{43}C_{44}H_{76}$ have different binding energies in various substitutional and interstitial defects. The maximum binding energy of the oxygen at carbon substitutional defect is about −0.5 eV and at interstitial defect is −0.18 eV. The HOMO-LUMO gap of the pure $Si_{43}C_{44}H_{76}$ is about 6.71 eV and after doping with oxygen changes on the order of 0.1 eV. Our studies show that the refractive index of the doped $Si_{43}C_{44}H_{76}$ nanocrystal significantly dispersed in comparison with pure SiC nanocrystal especially at the range of 6 to 8 eV.

Keywords Nanocrystal · Optical property · Silicon carbide

Introduction

The study of the nanostructures has attracted great attention recently in the field of semiconductor research [1, 2]. Nanocrystal is one of the most common zero dimensional nanostructures and many kinds of materials can be synthesized into nanocrystal structures. It is well know that SiC based materials are promising for substitution of silicon in electronic industry due to the great potential applications in high frequency, high temperature and radiation-resistant electronic devices [3, 4].

So far numerous reports have demonstrated synthesis of SiC nanostructures [5–11]. Embedded SiC nanocrystals could be used as environmentally friendly nano-optics [12–14]; also they have been studied extensively in the last 10 years as very interesting object for potential application as nano-scale light emitters for blue and UV spectral ranges [15–17]. Moreover they are one of the best candidates for biomarkers [18, 19].

Recently some of research works have been concentrated theoretically on the physical or chemical properties of SiC nanostructures [20, 21]. So far some theoretical aspects of the SiC nanotubes (SiCNTs) have been reported in the literature [22, 23]. The stability and electronic structures of SiCNTs were studied with the *ab initio* method. The results show that single-walled SiCNTs are wide band-gap semiconductors and their gap is independent of their helicity and radius. Also SiCNT are more suitable than bulk SiC in the application of nano-electronic devices [24].

In addition to the shape and size controlling of the materials in the nano-scale range, the incorporation of atomic impurities is a common way to modify the physical properties of a nanostructure. In this work we study a typical hydrogen-passivated cubic SiC nanocrystal ($Si_{43}C_{44}H_{76}$) using the density functional theory (DFT) based on the pesudopotential linear combination of atomic orbitals with super-cell technique. We focus on the electronic structure, energy gap evolution and optical properties of the fluorine and oxygen doped-SiC nanocrystal.

This work is organized as follows: in section "Simulation methods", the theoretical framework we use is briefly described, while section "Results and discussions" and Conclusions are devoted to the discussion of the results concerning the electronic, optical properties and our conclusions, respectively.

M. Bezi Javan (✉)
Physics Department, Faculty of Sciences,
Golestan University, Gorgan, Iran
e-mail: javan.masood@gmail.com

M. Bezi Javan
e-mail: m.javan@gu.ac.ir

Simulation methods

Computational details

We study a typical spherical SiC nanocrystal with a diameter of 1.2 nm ($Si_{43}C_{44}H_{76}$) using linear combination atomic orbital (LCAO) in combination with pesudopotential density functional calculation. In total energy and density of states calculations, the double zeta basis set with polarization function was employed [25]. Our simulated nanocrystal have been modeled taking all the bulk 3C-SiC atoms contained within a sphere of a given radius of about 6 Å and terminating the surface dangling bonds with hydrogen atoms. So the nanocrystal has semispherical shape as shown in Fig. 1. The structural properties have been determined by allowing all the atoms of each SiC nanocrystal to fully relax. It is worth pointing out that the starting prototype nanocrystal has T_d symmetry. The SiC nanocrystal has been embedded in a large supercell in order to prevent interactions between the periodic replicas (about 30 Å of vacuum separate) neighboring nanocrystals in all the considered systems. Full geometry optimization was performed with *ab initio* calculations based on the generalized gradient approximation (GGA) with the Perdew-Burke-Ernzerhof (PBE) functional [26] in the density functional theory (DFT) and standard norm-conserving Troullier-Martins Pseudo-potentials [27]. A cutoff of 120 Ry for the grid integration was used to represent the charge density. The total energy of the molecular system and Hellman-Feynman forces acting on atoms were calculated with convergence tolerance set to 10^{-4} eV and 0.05 eV $Å^{-1}$, respectively.

Theoretical description

In this work we extend the optical response calculations to take into account the effect of the fluorine and oxygen as impurity atoms. We employed the results of our calculations with the optimal basis set to compute the dielectric function of examined SiC nanocrystal. It is well known that the electric field of the incoming light can polarize the materials using the following relation [28]:

$$P^i(\omega) = X_{ij}^{(1)}(-\omega,\omega)\cdot E^j(\omega), \tag{1}$$

where $\chi_{ij}^{(1)}$ is the linear optical susceptibility tensor which is directly proportional to the product of the moment matrix elements between pairs of occupied valence (n) and unoccupied conduction (m) bands and inversely proportional to the transition energy.

It is given by [29]:

$$X_{ij}^{(1)}(-\omega,\omega) = \frac{e^2}{\hbar\Omega}\sum_{nm\,\vec{k}} f_{nm}\left(\vec{k}\right)\frac{r_{nm}^i\left(\vec{k}\right)r_{mn}^i\left(\vec{k}\right)}{\omega_{nm}\left(\vec{k}\right)-\omega} = \frac{\varepsilon_{ij}(\omega)-\delta_{ij}}{4\pi} \tag{2}$$

In the above relation, the n and m indicate energy bands, $f_{mn}\left(\vec{k}\right)\equiv f_m\left(\vec{k}\right)-f_n\left(\vec{k}\right)$ is the Fermi occupation factor, Ω is the unit cell volume, i.e., $(\Omega=a.(b\times c))$. In our work, the SiC nanocrystal located at the center of supercell has a

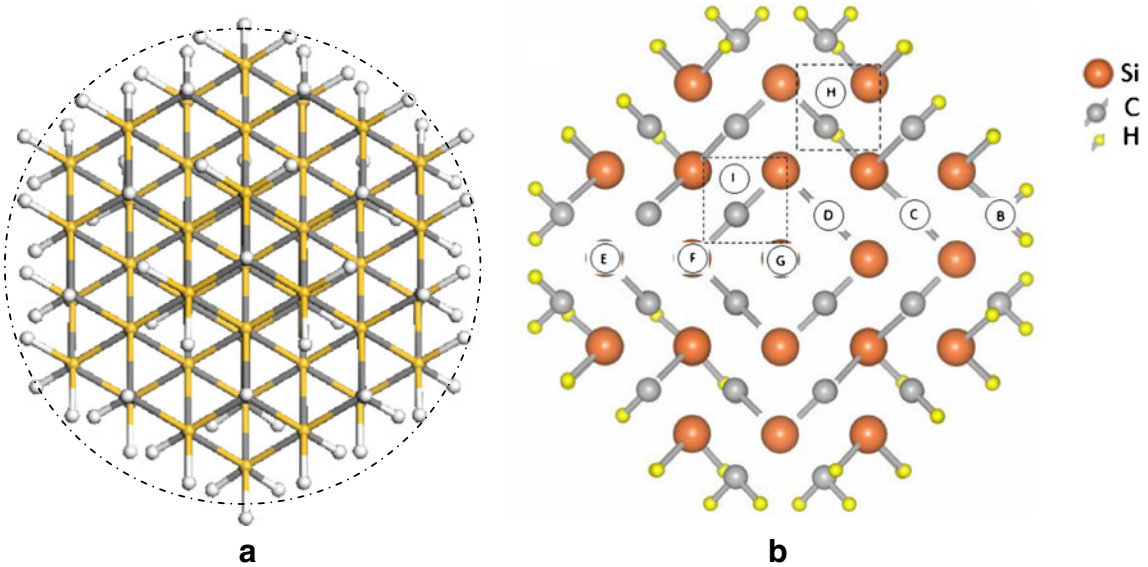

Fig. 1 **a** The optimized geometry of the $Si_{43}C_{44}H_{76}$ nanocrystal, **b** schematic cross sectional configuration of the $Si_{43}C_{44}H_{76}$ and different symmetrical situation where an impurity placed in the nanocrystal lattice (carbon or silicon substitutional defects) or between different layers (interstitial sites) in our calculations

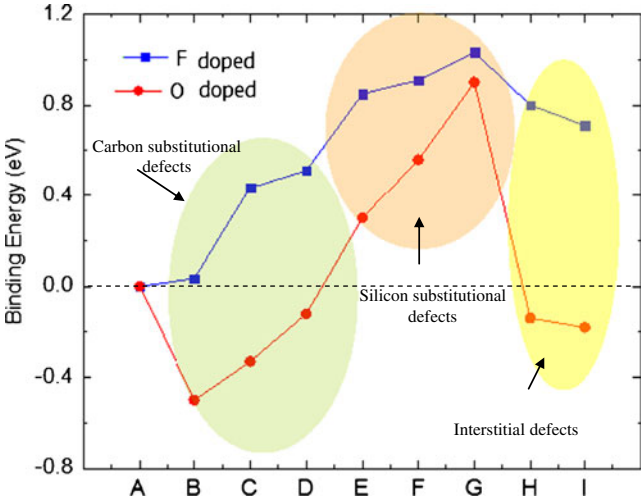

Fig. 2 The fluorine and oxygen binding energy to the SiC nanocrystal in different schemes

volume of 1.72 nm^3 (a=b=c=1.2 nm). $\omega_{mn}\left(\vec{k}\right)\equiv\omega_m\left(\vec{k}\right)-\omega\left(\vec{k}\right)$ is the frequency differences. The $\vec{r}_{mn}$ is the matrix elements of the position operator and are give by

$$r^i_{nm}\left(\vec{k}\right)=\begin{cases}\dfrac{v^i_{nm}(k)}{i\omega_{nm}}; & \omega_n\neq\omega_m\\ 0 & \omega_n=\omega_m\end{cases}, \tag{3}$$

where $v^i_{nm}\left(\vec{k}\right)=m^{-1}p^i_{nm}\left(\vec{k}\right)$, m is the free electron mass, and $\vec{p}_{nm}$ is the momentum matrix element. According to the above relations the dielectric function is defined as:

$$\varepsilon_{ij}(\omega)=1+4\pi\chi^{(1)}_{ij}(-\omega,\omega). \tag{4}$$

The imaginary part (ε_2) of the dielectric function can be obtained by:

$$\varepsilon^{ij}_2(\omega)=\frac{e^2}{\hbar\pi}\sum_{nm}\int d\vec{k}\,f_{nm}\left(\vec{k}\right)\frac{v^i_{nm}\left(\vec{k}\right)v^j_{nm}\left(\vec{k}\right)}{\omega^2_{mn}}\delta\left(\omega-\omega_{nm}\left(\vec{k}\right)\right). \tag{5}$$

Using the Kramers-Kroning transformation the real part of the dielectric function can be expressed by:

$$\varepsilon^{ij}_1(\omega)=\frac{2}{\pi}P\int_0^\infty\frac{\omega'\varepsilon^{ij}_2(\omega')}{\omega'^2-\omega^2}d\omega'. \tag{6}$$

The optical response of the hydrogen-terminated SiC nanocrystals was implemented in SIESTA [30]. The optical matrix element was calculated including the corrections due to the nonlocality of the pesudopotential [31]. The refractive index, n, the optical absorption coefficient, and energy-loss spectrum then can be calculated by the following formula [32]:

$$n=\sqrt{\frac{\sqrt{\varepsilon_1^2(\omega)+\varepsilon_2^2(\omega)}+\varepsilon_1(\omega)}{2}}, \tag{7}$$

$$\alpha=2\frac{\omega}{c}\sqrt{\frac{\sqrt{\varepsilon_1^2(\omega)+\varepsilon_2^2(\omega)}-\varepsilon_1(\omega)}{2}}. \tag{8}$$

Results and discussions

To eliminate the extra interacting with nanocrystal surface, the surface dangling bonds have been terminated by hydrogen atoms so we have $Si_{43}C_{44}H_{76}$ nanocrystal with approximate diameter of 1.25 nm. In Fig. 1(a) the optimized geometry of the $Si_{43}C_{44}H_{76}$ is shown which is taken from minimizing of the Hellmann-Feynman force calculated by DFT-PBE approach and LCAO level of theory. The average C-H and Si-H bond lengths in $Si_{43}C_{44}H_{76}$ are 1.15 and 1.49 Å. In the case of the Si-C bond, the inner bond lengths are about 1.85 Å while the bonds near the nanocrystal surface are about 1.91 Å, which is compatible with LDM-PM3 calculation [20].

Regarding this fact that an impurity can substitute or place in different positions of the nanocrystal lattice, in Fig. 1(b) we have shown a cross section of the $Si_{43}C_{44}H_{76}$ configuration where the impurities (fluorine and oxygen atoms) positions in different calculations were assigned by the capital letters from **B** to **I**. We also named **A**, the pure $Si_{43}C_{44}H_{76}$ nanocrystal. In **B**, **C** and **D** systems one carbon atom of the $Si_{43}C_{44}H_{76}$ nanocrystal is replaced by an impurity atom (carbon substitutional defect) while in **E**, **F** and **G** systems a silicon atom of the nanocrystal is replaced by an impurity atom (silicon substitutional defect). In the cases of **H** and **I** systems, the impurities place between different layers of the nanocrystal which have different distances from the nanocrystal center (interstitial sites).

One of the most important quantities which indicates the chemical stability of the complexes is the binding energy. The binding energy can be defined as the difference between the total energy of the system and the sum of all isolated atom energies which exist in the system. The negative sign of the binding energy means that the complexes are energetically favorable and one can expect that these complexes really form stable structures in experimental conditions. In Fig. 2 we have shown the binding energies of the fluorine and oxygen impurities in different situations of defects. As is seen from the figure, the carbon substitutional and interstitial defects are energetically favorable for oxygen impurity

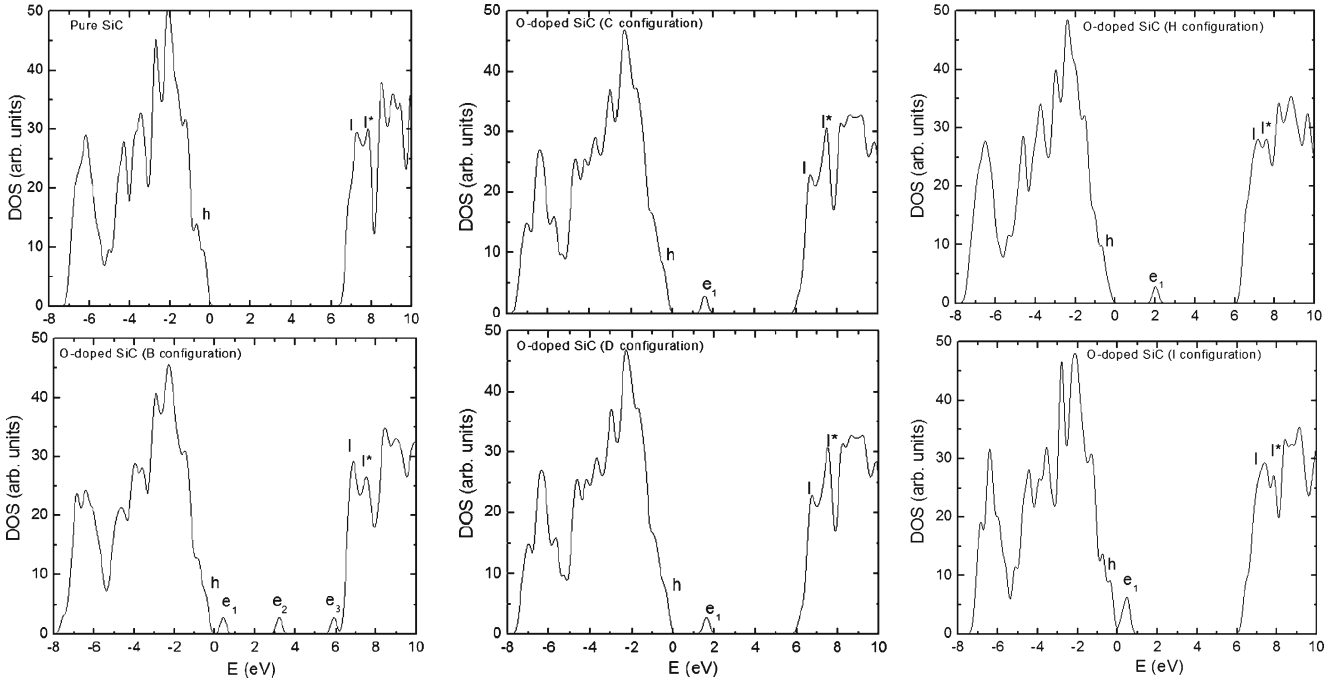

Fig. 3 The total density of state of the stable doped SiC nanocrystals. The 'h', 'l', 'e' and the 'l*' indicate the HOMO, LUMO, impurity state and nearest DOS peak to the LUMO level of the nanocrystals, respectively

unlike the silicon substitutional defects. It is also seen for **B** to **D** configuration of O-doped SiC nanocrystal the amount of the binding energy of the oxygen atom decreases when it gets close to the nanocrystal center. The value of the binding energy for **B**, **C**, **D**, **H** and **I** are −0.50, −0.33, −0.12, −0.14 and −0.18 eV, respectively. In the case of the F-doped SiC nanocrystal, the binding energy of the fluorine in all examined situation are positive although the binding energy of the fluorine in the surface carbon substitutional defect are significantly close to zero, which means that the fluorine doped SiC nanocrystal is an energetically unfavorable system. According to the considered results of the binding energy curves we follow the electronic and optical properties of the most stable oxygen doped SiC nanocrystals.

For further investigation, the electronic density of states (DOS) of the most stable O-doped $Si_{43}C_{44}H_{76}$ nanocrystal are discussed and in Fig. 3. For further evolution, the highest occupied molecular orbital (HOMO), lowest unoccupied molecular orbital (LUMO) and impurity states are shown by 'h', 'l' and indexed 'e' characters. Also the 'l*' indicate the nearest peak to the LUMO level of the doped nanocrystals. In general, single impurities can deform significantly the electronic configuration of the systems containing a few atoms. The most important role of the impurities in semiconducting systems is the appearance of the new electronic states in the band gap. As can be seen from the figure, the $Si_{42}NC_{44}H_{76}$ nanocrystal has a wide band gap about 6.71 eV. In the case of **B** configuration of the O-doped SiC nanocrystal the HOMO-LUMO gap has no significant change but three peaks of e_1, e_2 and e_3 appear in the gap region. The first two peaks of e_1 and e_2 are strongly localized on oxygen atomic states but the e_3 peak is related to the surface electronic states of the SiC nanocrystal. For **C**, **D**, **H**, and **I** configurations, the HOMO-LUMO gap of the doped nanocrystals has a small changes but in all cases an impurity state peak (e_1) appears in the gap region. As is clear from the figure, the location of the peak is strongly related to the doping condition. It is also seen that for carbon substitutional defects, the DOS of the nanocrystal especially for **C** and **D** configurations of doping is the same although the binding energy of the oxygen atom has a difference of about 0.2 eV for these two configurations. We have listed the impurity

Table 1 The energy gap (eV) between HOMO (h), LUMO (l) and impurity energy levels (e) in various configurations of oxygen doped SiC nanocrystal. The l^* is the first DOS peak near the LUMO energy level

System			
A (pure SiC-nc)	h-l (6.71)	h-l^*(7.80)	
B (O-doped SiC-nc)	h-l (6.84)	h-l^*(7.51)	h-e_1 (0.51)
			h-e_2 (3.25)
			h-e_3 (5.95)
C (O-doped SiC-nc)	h-l (6.69)	h-l^* (7.48)	h-e_1 (1.58)
D (O-doped SiC-nc)	h-l (6.75)	h-l^* (7.51)	h-e_1 (1.61)
H (O-doped SiC-nc)	h-l (6.88)	h-l^* (7.69)	h-e_1 (1.99)
I (O-doped SiC-nc)	h-l (6.75)	h-l^* (7.85)	h-e_1 (0.47)

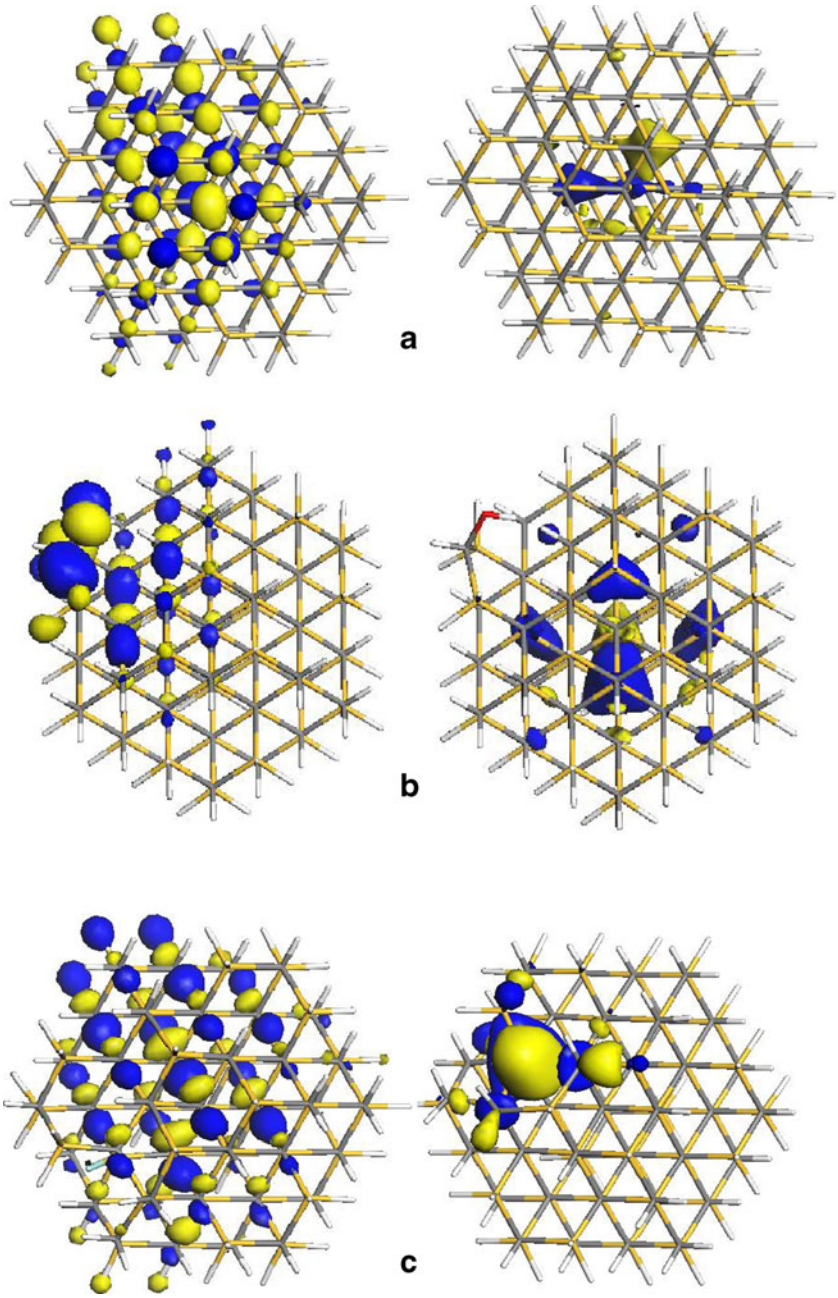

Fig. 4 the HOMO (left) and LUMO (right) wave function of the various O-doped $Si_{43}C_{44}H_{76}$ nanocrystals

DOS peaks of the various systems of doping in Table 1, the positions of the peaks relative to the upper edge of the valence band are presented. In Fig. 4, the contribution of the HOMO and LUMO wave function for most stable oxygen doped $Si_{43}C_{44}H_{76}$ nanocrystals are shown. With comparison of the HOMO and LUMO wave function of the pure and doped system, we can see the LUMO of the **C**, **D**, **H**, and **I** configurations significantly affected by oxygen impurity as the LUMO wave function especially localized on the oxygen atom, while in the case of the **B** configuration the HOMO is significantly disturbed and the LUMO has small variations.

According to the changes in the electronic states of the $Si_{43}C_{44}H_{76}$ nanocrystal due to doping with fluorine and oxygen atoms, the changes in optical properties of the nanocrystal is unavoidable. The optical absorptions of the pure and various most stable O-doped $Si_{43}C_{44}H_{76}$ nanocrystals are shown in Fig. 5. We have shown the main peaks of the absorption spectrum of the various doped SiC nanocrystals on the figures by a_1, a_2, and a_3 symbols. It can be found that there is strong correlation between optical absorption, refractive index and energy gap region properties of the nanocrystals. In Table 2, the correlation between DOS and

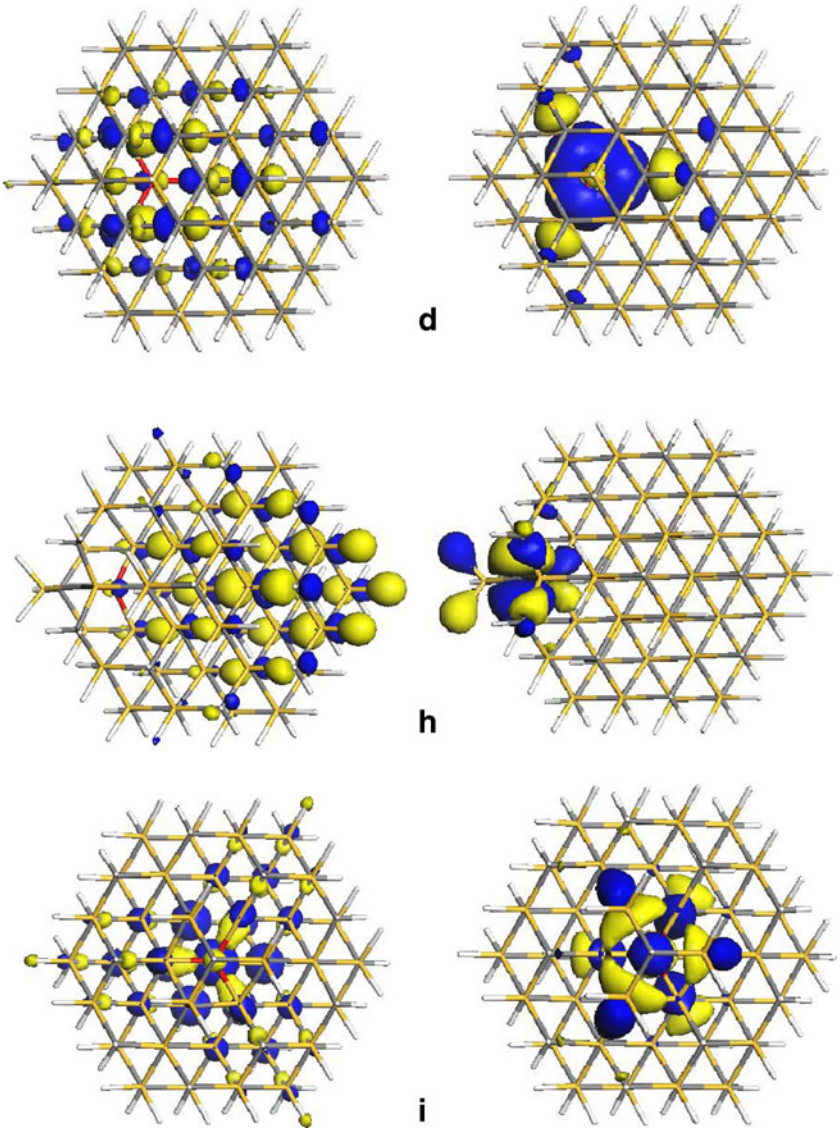

Fig. 4 (continued)

optical absorption main peak were summarized. Generally, in all absorption curves, a sizable peak exists at the range of 6–8 eV. As seen from the figure in pure $Si_{43}C_{44}H_{76}$, this peak corresponds to the vertical electronic excitations from h→l and h→l* which we index with a_1 and a_2, respectively. For **B** configuration five distinct peaks appear in the absorption spectrum. The a_1 (6.57 eV) and a_2 (7.02 eV) are related to the h→l and h→l* vertical excitations and the a_3 (5.05 eV), a_4 (3.78 eV) and a_5 (2.79 eV) correspond to the h→e_3, e_1→e_3, both h and e1→e_2 vertical excitations, respectively. For **C** and **D** configurations four peaks appear in the absorption spectrum. The a_1 (6.57 eV) and a_2 (6.97 eV) are related to the h→l and h→l* vertical excitations and the a_3 (5.01 eV) and a_4 (4.58 eV) correspond to the a_3 (e_1→l*) and a_4 (e_1→l) vertical excitations, respectively.

For **H** configuration two main peaks appear in the absorption spectrum. The a_1 (7.19 eV) which is related to the h→l and h→l* vertical excitations and a_2 (4.46 eV) that correspond to the a_3 (e_1→l and l*) vertical excitations, respectively. In the case of the **H** configuration, h→l and h→l* vertical excitations are completely distinct together and the a_3 (0.68 eV) peak refer to h→e_1 transition.

More of the studied refractive indexes of the O-doped $Si_{43}C_{44}H_{76}$ nanocrystal are shown in Fig. 6. It is easily seen that the static refractive index for all configurations of the oxygen doped systems are about 2.65, which is significantly close to the bulk 3C-SiC structre. Also, It can be seen from the figure that the incident photon significantly disperses by pure SiC nanocrystal especially in the light energy range of 6 to 8 eV. It is also found that in the case of O-doped systems

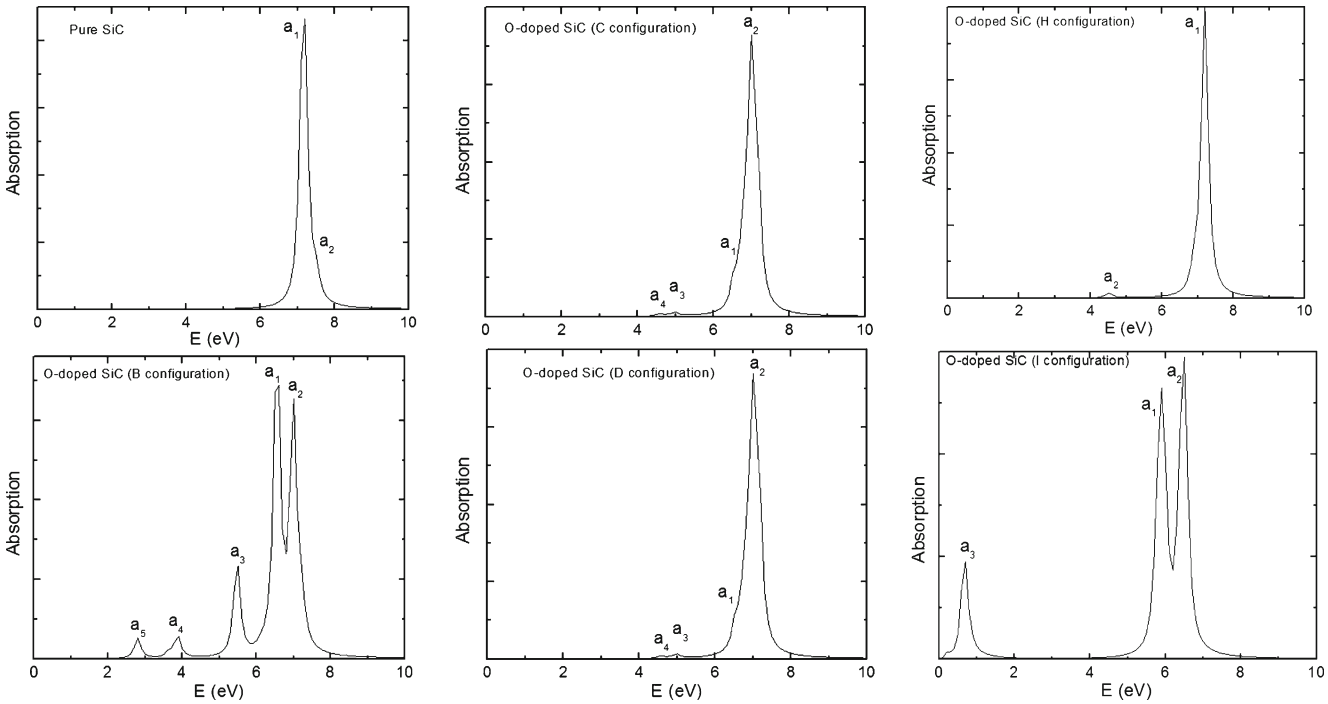

Fig. 5 The calculated absorption coefficient of $Si_{43}C_{44}H_{76}$ nanocrystal in various O-doped configurations

the refractive index dispersion is strongly correlated with DOS of the systems. The main dispersion peaks shift toward a lower energy region of light especially in the surface doping of oxygen impurity or **B** configuration.

Conclusions

We have studied a typical spherical SiC nanocrystal with a diameter of 1.2 nm ($Si_{43}C_{44}H_{76}$) using linear combination of atomic orbitals in combination with pesudopotential density functional calculation. The role of fluorine and oxygen impurities was investigated on the electronic and optical properties of the $Si_{43}C_{44}H_{76}$ nanocrystal. Total energy calculations show that the fluorine and oxygen have different binding energies in various substitutional and interstitial defects. We found that the oxygen can bind to the SiC nanocrystal especially in the carbon substitutional defects and also interstitial defects. The maximum binding energy of the oxygen at carbon substitutional defect is about −0.5 eV and at interstitial defect is −0.18 eV. We also

Table 2 The main optical transitions between HOMO (h), LUMO (l) and impurity energy levels in various configurations of O-doped-SiC nanocrystals

System			
A (pure SiC-nc)	a_1 (h→l)	a_2 (h→l^*)	
B (O-doped SiC-nc)	a_1(h→l)	a_2 (h→l^*)	a_3(h→e_3 and e_1→e_3)
			a_4(h→e_2)
			a_5(e_1→e_2)
C (O-doped SiC-nc)	a_1 (h→l)	a_2 (h→l^*)	a_3(e_1→l^*)
			a_4(e_1→l)
D (O-doped SiC-nc)	a_1 (h→l)	a_2 (h→l^*)	a_3(e_1→l^*)
			a_4(e_1→l)
H (O-doped SiC-nc)	a_1 (h→l and (h→l^*))		a_2 (e_1→l)
I (O-doped SiC-nc)	a_1 (h→l)	a_2 (h→l^*)	a_3(h→e_1)

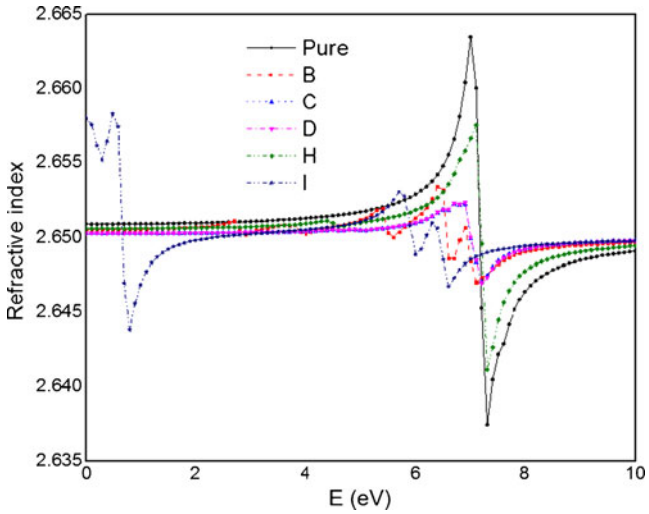

Fig. 6 The calculated refractive index of $Si_{43}C_{44}H_{76}$ nanocrystal in various O-doped configurations

found that the fluorine doped $Si_{43}C_{44}H_{76}$ nanocrystal is an unstable system. The HOMO-LUMO gap of the pure $Si_{43}C_{44}H_{76}$ is about 6.71 eV and after doping with oxygen changes on the order of 0.1 eV. Our studies show that the refractive index of the doped $Si_{43}C_{44}H_{76}$ nanocrystal significantly dispersed in comparison with pure SiC nanocrystal especially at the range of 6 to 8 eV. However, the static refractive index of the $Si_{43}C_{44}H_{76}$ nanocrystal is significantly close to the bulk 3C-SiC (2.55).

References

1. Rurali R (2005) Electronic and structural properties of silicon carbide nanowires. Phys Rev B 71:205405–205412
2. Bekaroglu E, Topsakal M, Cahangirov S, Ciraci S (2010) First-principles study of defects and adatoms in silicon carbide honeycomb structures. Phys Rev B 81:075433–075442
3. Chelnokov VE, Syrkin AL, Dmitriev VA (1997) Overview of SiC power electronics. Diam Relat Mater 6:1480–1484
4. Zolper JC, Skowronski M (2005) Advances in silicon carbide electronics. MRS Bull 30:273–278
5. Deokar G, Angelo MD, Cavellin CD (2011) Synthesis of 3C-SiC nanocrystals at the SiO_2/Si interface by CO2 thermal treatment. J Nanosci Nanotechno 11:9232–9238
6. Weishart H, Heera V, Eichhorn F, Pecz B, Barna A, Skorupa W (2003) Ion beam synthesis of diamond-SiC-heterostructures. Diam Relat Mater 12:1241–1245
7. Zhokhov AA, Masalov VM, Matveev DV, Maksimuk MY, Zver'kova II, Khasanov SS, Shmurak SZ, Kiselev AP, Bazhenov AV, Emel'Chenko GA (2009) Synthesis of α-SiC nanocrystals by carbothermal reduction of spherical nanoparticles of amorphous silicon dioxide. Phys Solid State 51:1723–1729
8. Selvan ST, Aldeyab SS, Zaidi SMJ, Arivuoli D, Ariga K, Mori T, Vinu A (2011) Morphological control of porous SiC templated by As-synthesized form of mesoporous silica. J Nanosci Nanotech 11:6823–6832
9. Schubert C, Kaiser U, Hedler A, Wesch W, Gorelik T, Glatzel U, Kraublich J, Wunderlich B, Heb G, Goetz K (2002) Nanocrystal formation in SiC by Ge ion implantation and subsequent thermal annealing. J Appl Phys 91:1520–1525
10. Ting L, Liqiang X, Liancheng W, Lishan Y, Yitai Q (2009) Synthesis and characterization of 3C and 2H-SiC nanocrystals starting from SiO2, C2H5OH and metallic Mg. J Alloys Comp 484:341–346
11. Huang ZR, Liang B, Jiang DL, Tan SH (1996) Preparation of nanocrystal SiC powder by chemical vapour deposition. J Mater Sci 31:4327–4332
12. Reboredo F, Pizzagalli L, Galli G (2004) Computational engineering of the stability and optical gaps of the SiC quantum dots. Nano Lett 4:801–805
13. Makkai Z, Pécz B, Bársony I, Vida G, Pongrácz A, Josepovits KV, Deák P (2005) Isolated SiC nanocrystals in SiO_2. Appl Phys Lett 86:253109–253112
14. Peng XH, Nayak SK, Alizadeh A, Varanasi KK, Bhate N, Rowland LB, Kumar SK (2007) First-principles study of the effects of polytype and size on energy gaps in SiC nanoclusters. J Appl Phys 102:024304–024309
15. Matsumoto T, Takahashi J, Tamaki T, Futagi T, Mimura H, Kanemitsu Y (1994) Blue–green luminescence from porous silicon carbide. Appl Phys Lett 64:226–229
16. Liao LS, Bao XM, Yang ZF, Min NB (1995) Intense blue emission from porous β–SiC formed on C^+–implanted silicon. Appl Phys Lett 66:2382–2385
17. Torchynska TV, Diaz Cano A, Jimenez Sandoval S, Dybic M, Ostapenko S, Mynbaeva M (2005) Photoluminescence and Raman spectroscopy in porous SiC. Microelectronics 36:536–538
18. Botsoa J, Lysenko V, Géloën A, Marty O, Bluet JM, Guillot G (2008) Application of 3*C*-SiC quantum dots for living cell imaging. Appl Phys Lett 92:173902–173905
19. Fan J, Li H, Jiang J, So LKY, Lam YW, Chu PK (2008) 3C–SiC Nanocrystals as Fluorescent Biological Labels. Small 4:1058–1060
20. Shi SL, Xu SJ, Wang XJ, Chen GH (2006) Theoretical absorption spectra of silicon carbide nanocrystals. Thin Solid Films 495:404–406
21. Voros M, Deak P, Frauenheim T, Gali A (2010) The absorption spectrum of hydrogenated silicon carbide nanocrystals from *ab initio* calculations. Appl Phys Lett 96:051909–051912
22. Miyamoto Y, Yu BD (2002) Computational designing of graphitic silicon carbide and its tubular forms. Appl Phys Lett 80:586–588
23. Gali A (2006) *Ab initio* study of nitrogen and boron substitutional impurities in single-wall SiC nanotubes. Phys Rev B 73:245415–245424
24. Zhao MW, Xia YY, Li F, Zhang RQ, Lee ST (2005) Strain energy and electronic structures of silicon carbide nanotubes: density functional calculations. Phys Rev B 71:085312–085318
25. Artacho E, Sancez-Potal D, Ordejon P, Garcia A, Soler J (1999) Linear scaling ab initio calculations for large and complex systems. Phys Status Solidi B 215:809–817
26. Perdew JP, Burke S, Ernzerhof M (1999) Generalized gradient approximation made simple. Phys Rev Lett 77:3865–3868
27. Troullier N, Martins JL (1991) Efficient pseudopotentials for plane-wave calculations. Phys Rev B 43:1993–2006
28. Levine ZH, Allan DC (1989) Linear optical response in silicon and germanium including self-energy effects. Phys Rev Lett 63:1719–1722
29. Philipp H, Ehrenreich RH (1963) Optical properties of semiconductors. Phys Rev 129:1550–1560
30. Soler JM, Artacho E, Gale JD, Garcia A, Junquera J, Or-dejon P, Sanchez-Portal D (2002) The SIESTA method for ab initio order-N materials simulation. J Phys Condens Matter 14:2745–2779
31. Read AJ, Needs RJ (1991) Calculation of optical matrix elements with nonlocal pseudopotentials. Phys Rev B 44:13071–13073
32. Griffiths DJ (1999) Introduction to electrodynamics. Prentice Hall, Englewood Cliffs